energies

MDPI

*Article*

# Nonlinear Observer-Based Robust Passive Control of Doubly-Fed Induction Generators for Power System Stability Enhancement via Energy Reshaping

**Jun Dong [1], Shengnan Li [2], Shuijun Wu [2], Tingyi He [2], Bo Yang [3], Hongchun Shu [3,*] and Jilai Yu [1]**

[1] School of Electrical Engineering and Automation, Harbin Institute of Technology, Harbin 150001, China; dongjun_kust@sina.com (J.D.); yupwrs@hit.edu.cn (J.Y.)
[2] Faculty of Electric Power Engineering, Kunming University of Science and Technology, Kunming 650500, China; lsn788@sina.com (S.L.); yepri_wsj@126.com (S.W.); htyfish@163.com (T.H.)
[3] Electric Power Research Institute of Yunnan Power Grid Co., Ltd., Kunming 650217, China; yangbo_ac@outlook.com
* Correspondence: kmshc@sina.com

Received: 20 May 2017; Accepted: 21 July 2017; Published: 25 July 2017

**Abstract:** The large-scale penetration of wind power might lead to degradation of the power system stability due to its inherent feature of randomness. Hence, proper control designs which can effectively handle various uncertainties become very crucial. This paper designs a novel robust passive control (RPC) scheme of a doubly-fed induction generator (DFIG) for power system stability enhancement. The combinatorial effect of generator nonlinearities and parameter uncertainties, unmodelled dynamics, wind speed randomness, is aggregated into a perturbation, which is rapidly estimated by a nonlinear extended state observer (ESO) in real-time. Then, the perturbation estimate is fully compensated by a robust passive controller to realize a globally consistent control performance, in which the energy of the closed-loop system is carefully reshaped through output feedback passification, such that a considerable system damping can be injected to improve the transient responses of DFIG in various operation conditions of power systems. Six case studies are carried out while simulation results verify that RPC can rapidly stabilize the disturbed DFIG system much faster with less overshoot, as well as supress power oscillations more effectively compared to that of linear proportional-integral-derivative (PID) control and nonlinear feedback linearization control (FLC).

**Keywords:** robust passive control; nonlinear observer; stability enhancement; energy reshaping

## 1. Introduction

In recent years, the ever-growing global interest in renewable energy resources is attracting enormous attention from both industry and academics due to the worldwide increase in power demand, as well as the limitation of fossil fuels and their harmful impact on the environment. Sustainable energy resources, such as wind, solar, tidal, biomass, etc., are naturally abundant, clean and have a much less harmful impact on the environment than fossil fuels [1]. Meanwhile, an enormous variety of large-scale renewable energy has been integrated into the smart grid [2], while the issue of management and energy shaping of demand side has been well addressed by the use of multi-agent systems in smart distribution [3]. Nowadays, doubly-fed induction generator (DFIG) has been widely employed into wind farm thanks to its merits of decoupled control of active/reactive power and partial-scale converters [4]. The dramatic increase of high-percentage wind energy penetration represents a great challenge in power system stability, which may cause active power and reactive power oscillations [5]. Moreover, [6] reported a Hopf bifurcation control of power systems nonlinear dynamics via a dynamic state feedback controller. Besides, the security

and privacy issues of smart grids become very crucial [7]. As a consequence, proper control design of DFIGs is very crucial and urgent to enhance the power system stability.

Generally speaking, conventional proportional-integral-derivative (PID) control parameters are determined by one-point linearization of the original nonlinear system, thus its control performance might be degraded when operation conditions vary significantly [8]. This issue becomes quite severe in DFIGs as they are strongly nonlinear due to the aerodynamics of wind turbines, together with the highly stochastic wind speed. Therefore, more advanced control designs for DFIG needs to be developed to handle such difficult problems.

So far, many parameter tuning methods have been used to obtain the optimal control parameters of DFIG in several given scenarios, e.g., genetic algorithm (GA) [9] was employed to search the optimal parameters of gain scheduling controller for rotor side converter (RSC) of DFIG; particle swarm optimizer (PSO) [10] was adopted to ensure an maximum power point tracking (MPPT) of DFIG through an indirect power control, which leads to a less error criteria of performance index compared with that of the manually tuned PID controller; grouped grey wolf optimizer (GGWO) [11] was proposed to optimally extract the wind energy by mimicking the hunting strategy and social hierarchy of wild grey wolf groups, etc.

On the other hand, a large number of nonlinear or robust control schemes have been investigated to handle the above obstacles, which are able to naturally avoid the inherent weakness of PID control. In [12], a feedback linearization control (FLC) was developed to globally compensate the nonlinearities of DFIGs while the internal dynamics stability is analysed in the sense of Lyapunov criteria; In addition, a high-order sliding-mode control (SMC) was applied which owns prominent advantages of great robustness against to different types of power grid fault, together with no extra mechanical stress on the wind turbine drive train [13]. Besides, reference [14] designed a GA-based adaptive controller for DFIGs to improve the system damping. Moreover, a robust controller was proposed for stator active and reactive currents, which requires less machine parameters and robust against variation in the grid voltage amplitude [15].

In the energy-based nonlinear control theory, passivity provides a physical insight for the analysis and design of nonlinear systems, which decomposes a complex nonlinear system into simpler subsystems that, upon interconnection, adds up their local energies to determine the full system's behaviour. The action of a controller connected to the dynamical system may also be considered, in terms of energy, as another separate dynamical system. Hence, the control problem can then be treated as finding an interconnection pattern between the controller and the dynamical system. This "energy reshaping" approach is the essence of passive control (PC), also called passivity-based control (PBC), which takes into account the energy of the system and gives a clear physical meaning, such that the changes of the overall storage function can take a desired form [16–18]. PC has been successfully applied on resolving various complex engineering problems, such as graph-based power flow systems [19], collision avoidance for hub-beam spacecraft [20], stabilization of underactuated mechanical systems [21], multi-purpose droop control for electronically-interfaced distributed generators (DG) [22], and so on. However, one obvious drawback of PC is that an accurate system model is usually required, thus its applications are somehow limited.

However, the aforementioned approaches may have a quite complex structure which is difficult to implement in practice. Moreover, the physical meaning of DFIG is ignored during its control design. Also, they may merely be effective to just several types of uncertainties thus their application is somehow limited. The above three issues motivates this paper to design a more practical and widely applicable advanced controller with the consideration of the physical meaning of DFIG, which is called the robust passive control (RPC) to enhance the power system stability. So far, a variety of RPC has been studied, e.g., RPC which can achieve maximum dissipation of uncertain time-delay singular systems to deal with matrix inequalities and equality constraints [23], network based RPC for fuzzy systems to handle randomly occurring uncertainties, variable sampling intervals, and constant network-induced delay [24], robust observer-based passive control for uncertain singular time-delay system subject to actuator saturation [25], etc.

The contributions of this paper can be summarized in the following three points:

- The combinatorial effect of generator nonlinearities and parameter uncertainties, unmodelled dynamics, wind speed randomness, is aggregated into a perturbation, which is rapidly estimated by a nonlinear extended state observer (ESO), called sliding-mode state and perturbation observer (SMSPO) [26], in real-time. Hence, RPC can handle various types of uncertainties which is applicable to more practical cases compared to that of parameter based robust/adaptive approaches;
- RPC does not require an accurate DFIG model while only the active power and reactive power need to be measured. Thus, RPC is very easy to be implemented in practice;
- A great system damping can be injected to improve the transient responses of DFIG in various operation conditions of power systems via energy reshaping, which can provide a faster active power response when DFIG is disturbed thus the power system stability could be enhanced significantly.

Comprehensive case studies are carried out in order to evaluate its control performance against to two typical linear and nonlinear controllers. The remainder of this paper is organized as follows: Section 2 is devoted to DFIG modelling while Section 3 develops the RPC scheme. Then, Section 4 attempts to apply RPC on DFIG for power system stability enhancement. In Section 5, simulation results are presented. At last, some conclusions and possible future studies are summarized in Section 6.

## 2. System Modelling of DFIG-Based Wind Turbine

The configuration of a DFIG connected to a power grid is schematically illustrated in Figure 1. Here, an induction generator and a wind turbine are connected with a mechanical shaft system, which is directly connected to the power grid with its stator and a back-to-back converter with its rotor, respectively. The RSC controller aims to regulate the rotor speed and reactive power; while the grid side converter (GSC) controller attempts to maintain a constant DC link voltage from the variation of rotor power [11]. Note that the modelling of GSC is ignored as this paper focuses on active power regulation. As a consequence, only the RSC controller design is considered.

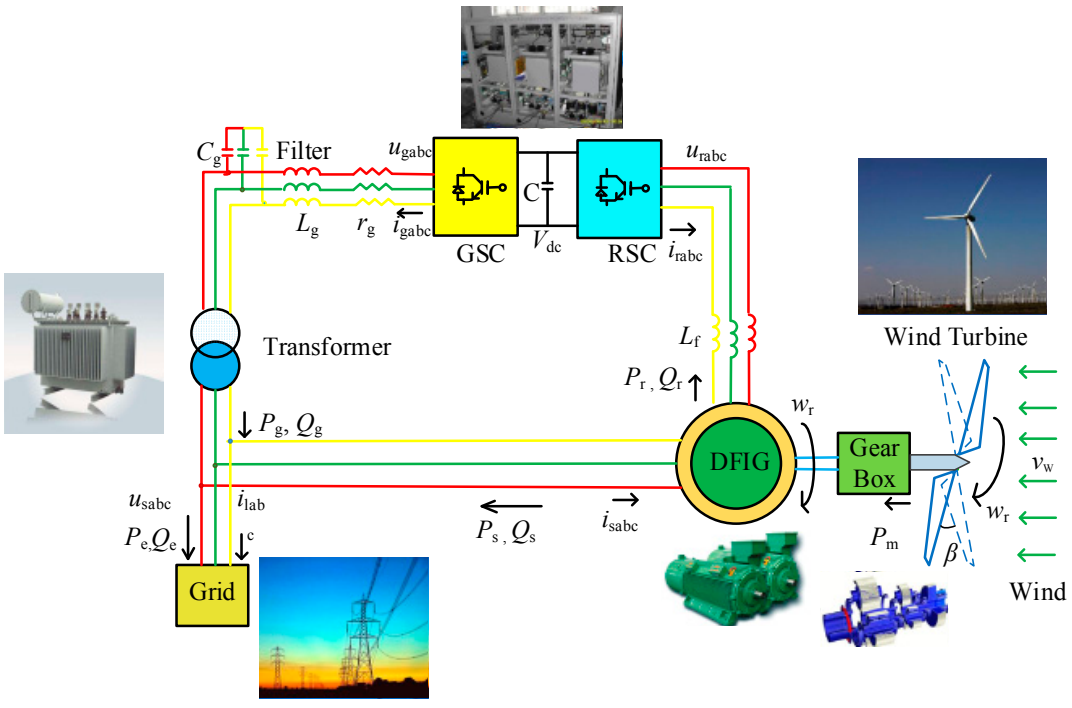


**Figure 1.** The configuration of a grid-connected DFIG-based wind turbine.

### 2.1. Wind Turbine Model

The mechanical power captured by wind turbine can be written as [12,27]:

$$P_{\mathrm{m}} = \frac{1}{2}\rho\pi R^2 C_{\mathrm{p}}(\lambda,\beta)v_{\mathrm{wind}}^3 \tag{1}$$

where $\rho$ is the air density, $R$ denotes the radius of wind turbine, and $v_{\mathrm{wind}}$ means the wind speed. $C_{\mathrm{P}}(\lambda,\beta)$ is a function of tip-speed-ratio $\lambda$ and blade pitch angle $\beta$ representing the power coefficient. A specific wind speed corresponds to a wind turbine rotational speed to obtain $C_{\mathrm{Pmax}}$, namely, the maximum power coefficient, and therefore tracks the maximum mechanical (wind) power. In general, the wind turbine operates in the variable speed mode if wind speed does not exceed its rated value, then the rotational speed is adjusted by DFIG speed control so that $C_{\mathrm{P}}(\lambda,\beta)$ can be remained at the $C_{\mathrm{Pmax}}$ point. However, if wind turbine operates above the rated wind speed, the pitch angle will be adjusted to guarantee the operation safety of the wind turbine. Finally, the tip-speed-ratio $\lambda$ can be defined as:

$$\lambda = \frac{\omega_{\mathrm{m}} R}{v_{\mathrm{wind}}} \tag{2}$$

where $\omega_{\mathrm{m}}$ denotes the wind turbine rotational speed. According to the wind turbine characteristics, a generic equation of $C_{\mathrm{P}}(\lambda,\beta)$ can be described by:

$$C_{\mathrm{p}}(\lambda,\beta) = c_1\left(\frac{c_2}{\lambda_i} - c_3\beta - c_4\right)e^{-\frac{c_5}{\lambda_i}} + c_6\lambda \tag{3}$$

with:

$$\frac{1}{\lambda_i} = \frac{1}{\lambda + 0.08\beta} - \frac{0.035}{\beta^3 + 1} \tag{4}$$

where $c_1$ to $c_6$ are set to: $c_1 = 0.5176$, $c_2 = 116$, $c_3 = 0.4$, $c_4 = 5$, $c_5 = 21$, and $c_6 = 0.0068$, respectively [12,27].

### 2.2. Generator Model

The generator dynamics is given by:

$$\begin{cases} \dfrac{\mathrm{d}i_{\mathrm{qs}}}{\mathrm{d}t} = \dfrac{\omega_{\mathrm{b}}}{L_{\mathrm{s}}^{'}}\left(-R_{\mathrm{l}}i_{\mathrm{qs}} + \omega_{\mathrm{s}}L_{\mathrm{s}}'i_{\mathrm{qs}} + \dfrac{\omega_{\mathrm{r}}}{\omega_{\mathrm{s}}}e_{\mathrm{qs}}' - \dfrac{1}{T_{\mathrm{r}}\omega_{\mathrm{s}}}e_{\mathrm{ds}}' - v_{\mathrm{qs}} + \dfrac{L_{\mathrm{m}}}{L_{\mathrm{rr}}}v_{\mathrm{qr}}\right) \\ \dfrac{\mathrm{d}i_{\mathrm{ds}}}{\mathrm{d}t} = \dfrac{\omega_{\mathrm{b}}}{L_{\mathrm{s}}^{'}}\left(-\omega_{\mathrm{s}}L_{\mathrm{s}}'i_{\mathrm{qs}} - R_{\mathrm{l}}i_{\mathrm{qs}} + \dfrac{1}{T_{\mathrm{r}}\omega_{\mathrm{s}}}e_{\mathrm{qs}}' + \dfrac{\omega_{\mathrm{r}}}{\omega_{\mathrm{s}}}e_{\mathrm{ds}}' - v_{\mathrm{ds}} + \dfrac{L_{\mathrm{m}}}{L_{\mathrm{rr}}}v_{\mathrm{qr}}\right) \\ \dfrac{\mathrm{d}e_{\mathrm{qs}}'}{\mathrm{d}t} = \omega_{\mathrm{b}}\omega_{\mathrm{s}}\left[R_2 i_{\mathrm{ds}} - \dfrac{1}{T_{\mathrm{r}}\omega_{\mathrm{s}}}e_{\mathrm{qs}}' + \left(1 - \dfrac{\omega_{\mathrm{r}}}{\omega_{\mathrm{s}}}\right)e_{\mathrm{ds}}' - \dfrac{L_{\mathrm{m}}}{L_{\mathrm{rr}}}v_{\mathrm{dr}}\right] \\ \dfrac{\mathrm{d}e_{\mathrm{ds}}'}{\mathrm{d}t} = \omega_{\mathrm{b}}\omega_{\mathrm{s}}\left[-R_2 i_{\mathrm{qs}} - \left(1 - \dfrac{\omega_{\mathrm{r}}}{\omega_{\mathrm{s}}}\right)e_{\mathrm{qs}}' - \dfrac{1}{T_{\mathrm{r}}\omega_{\mathrm{s}}}e_{\mathrm{ds}}' + \dfrac{L_{\mathrm{m}}}{L_{\mathrm{rr}}}v_{\mathrm{qr}}\right] \end{cases} \tag{5}$$

where $\omega_{\mathrm{b}}$ represents the electrical base speed, $\omega_{\mathrm{s}}$ denotes the synchronous angle speed, and $\omega_{\mathrm{r}}$ means the rotor angle speed; $e_{\mathrm{ds}}'$ and $e_{\mathrm{qs}}'$ denote the equivalent d-axis and q-axis (dq-) internal voltages; $i_{\mathrm{ds}}$ and $i_{\mathrm{qs}}$ are the dq-stator currents; $v_{\mathrm{ds}}$ and $v_{\mathrm{qs}}$ represent the dq-stator terminal voltages; $v_{\mathrm{dr}}$ and $v_{\mathrm{qr}}$ are the dq-rotor voltages. $L_{\mathrm{m}}$ means the mutual inductance; while the remaining parameters are provided in the Appendix A.

The active power $P_{\mathrm{e}}$ produced by the generator is calculated by:

$$P_{\mathrm{e}} = e_{\mathrm{qs}}'i_{\mathrm{qs}} + e_{\mathrm{ds}}'i_{\mathrm{ds}} \tag{6}$$

The q-axis is aligned with the stator voltage while the d-axis is aligned to lead the q-axis, thus, $v_{\mathrm{ds}} \equiv 0$ and $v_{\mathrm{qs}}$ equals to the terminal voltage magnitude.

The reactive power $Q_e$ is obtained as:

$$Q_e = v_{qs} i_{ds} - v_{ds} i_{qs} \tag{7}$$

*2.3. Shaft System Model*

The shaft system can be modelled as a single lumped-mass system, whose lumped inertia constant $H_m$ is calculated as [28]:

$$H_m = H_t + H_g \tag{8}$$

where $H_t$ and $H_g$ are the inertia constants of wind turbine and generator, respectively.

The electromechanical dynamics is written as:

$$\frac{d\omega_m}{dt} = \frac{1}{2H_m}(T_m - T_e - D\omega_m) \tag{9}$$

where $\omega_m$ represents the rotational speed of the lumped-mass system equivalent to the generator rotor speed $\omega_r$; $D$ denotes the lumped system damping; and $T_m$ is the mechanical torque with $T_m = P_m/\omega_m$, respectively.

## 3. Nonlinear Observer Based Robust Passive Control

Consider an uncertain nonlinear system which has the following canonical form:

$$\begin{cases} \dot{x} = Ax + B(a(x) + b(x)u + d(t)) \\ y = x_1 \end{cases} \tag{10}$$

where $x = [x_1, x_2, \cdots, x_n]^T \in R^n$ is the state variable vector; $u \in R$ and $y \in R$ are the control input and system output, respectively; $a(x)$: $R^n \mapsto R$ and $b(x)$: $R^n \mapsto R$ are unknown smooth functions; and $d(t)$: $R^+ \mapsto R$ represents a time-varying external disturbance. The $n \times n$ matrix $A$ and $n \times 1$ matrix $B$ are of the canonical form as follows:

$$A = \begin{bmatrix} 0 & 1 & 0 & \cdots & 0 \\ 0 & 0 & 1 & \cdots & 0 \\ \vdots & \vdots & \vdots & \vdots & \vdots \\ 0 & 0 & 0 & \cdots & 1 \\ 0 & 0 & 0 & \cdots & 0 \end{bmatrix}_{n\times n}, B = \begin{bmatrix} 0 \\ 0 \\ \vdots \\ 0 \\ 1 \end{bmatrix}_{n\times 1} \tag{11}$$

The perturbation of system (10) is defined as [16,26,29]:

$$\psi(x, u, t) = a(x) + (b(x) - b_0)u + d(t) \tag{12}$$

where $b_0$ is the constant control gain.

From the original system (10), the last state $x_n$ can be rewritten in the presence of perturbation (12), gives:

$$\dot{x}_n = a(x) + (b(x) - b_0)u + d(t) + b_0 u = \psi(x, u, t) + b_0 u \tag{13}$$

Define an extended state $x_{n+1} = \psi(x, u, t)$. Then, system (10) can be directly extended into:

$$\begin{cases} y = x_1 \\ \dot{x}_1 = x_2 \\ \vdots \\ \dot{x}_n = x_{n+1} + b_0 u \\ \dot{x}_{n+1} = \dot{\psi}(\cdot) \end{cases} \tag{14}$$

The new state vector becomes $x_e = [x_1, x_2, \cdots, x_n, x_{n+1}]^T$, and the following two assumptions are made [26,29]:

A.1 $b_0$ is chosen to satisfy $|\boldsymbol{b}(\boldsymbol{x})/\boldsymbol{b_0} - \mathbf{1}| \leq \boldsymbol{\theta} < \mathbf{1}$, where $\theta$ is a positive constant.

A.2 The function $\boldsymbol{\psi}(\boldsymbol{x},\boldsymbol{u},\boldsymbol{t})$: $\boldsymbol{R^n} \times \boldsymbol{R} \times \boldsymbol{R^+} \mapsto \boldsymbol{R}$ and $\dot{\boldsymbol{\psi}}(\boldsymbol{x},\boldsymbol{u},\boldsymbol{t})$: $\boldsymbol{R^n} \times \boldsymbol{R} \times \boldsymbol{R^+} \mapsto \boldsymbol{R}$ are bounded over the domain of interest $|\boldsymbol{\psi}(\boldsymbol{x},\boldsymbol{u},\boldsymbol{t})| \leq \boldsymbol{r_1}, |\dot{\boldsymbol{\psi}}(\boldsymbol{x},\boldsymbol{u},\boldsymbol{t})| \leq \boldsymbol{r_2}$ with $\boldsymbol{\psi}(\mathbf{0},\mathbf{0},\mathbf{0}) = \mathbf{0}$, and $\dot{\boldsymbol{\psi}}(\mathbf{0},\mathbf{0},\mathbf{0}) = \mathbf{0}$, where $\gamma_1$ and $\gamma_2$ are positive constants.

Throughout this paper $\tilde{x} = x - \hat{x}$ refers to the estimation error of $x$ whereas $\hat{x}$ represents the estimate of $x$, while $x^*$ denotes the reference of $x$. In the consideration of the worst case, e.g., $y = x_1$ is the only measurable state, an $(n + 1)$th-order SMSPO [26] for the extended system (14) is used to rapidly estimate all unmeasurable states and perturbation, as follows:

$$\begin{cases} \dot{\hat{x}}_1 = \hat{x}_2 + \alpha_1\tilde{x}_1 + k_1\mathrm{sat}(\tilde{x}_1, \epsilon_o) \\ \vdots \\ \dot{\hat{x}}_n = \hat{\psi}(\cdot) + \alpha_n\tilde{x}_1 + k_n\mathrm{sat}(\tilde{x}_1, \epsilon_o) + b_0u \\ \dot{\hat{\psi}}(\cdot) = \alpha_{n+1}\tilde{x}_1 + k_{n+1}\mathrm{sat}(\tilde{x}_1, \epsilon_o) \end{cases} \tag{15}$$

where $\alpha_i$, $i = 1, 2, \cdots, n + 1$, are the Luenberger observer gains which are chosen to place the poles of polynomial $s^{n+1} + \alpha_1 s^n + \alpha_2 s^{n-1} + \cdots + \alpha_{n+1} = (s + \lambda_\alpha)^{n+1} = 0$ being in the open left-half complex plane at $-\lambda_\alpha$, with $\alpha_i = C_{n+1}^i \lambda_\alpha^i$, $i = 1, 2, \cdots, n + 1$. In addition, positive gains $k_i$ are the sliding surface constants, in which $k_1 \geq |\tilde{x}_2|^{\max}$ must be chosen to guarantee that the estimation error of SMSPO (15) will enter into the sliding surface $S_{spo}(\tilde{x}) = \tilde{x}_1 = 0$, at $t > t_s$ and thereafter remain $S_{spo} = 0$, $t \geq t_s$. Due to the page limit and the scope of the journal, the proof of the existence and global stability of such sliding-mode mechanism, as well as the selection of small number $\epsilon_o$ can be referred to [30,31] for interested readers, which is based on Lyapunov theory. While the ratio $k_i/k_1$ ($i = 2, 3, \cdots, n + 1$) be chosen to put the poles of polynomial $p^n + (k_2/k_1)p^{n-1} + \cdots + (k_n/k_1)p + (k_{n+1}/k_1) = (p + \lambda_k)^n = 0$ to be in the open left-half complex plane at $-\lambda_k$. Meanwhile, it has $k_{i+1} = C_n^i \lambda_k^i \; k_1$, $i = 1,2,\cdots,n$. Moreover, $\mathrm{sat}(\tilde{x}_1, \epsilon_o)$ function is employed to replace the conventional $\mathrm{sgn}(\tilde{x}_1)$ function, such that the malignant effect of chattering usually existed in sliding-mode observers resulted from discontinuity can be reduced, which is defined as $\mathrm{sat}(\tilde{x}_1, \epsilon_o,) = \tilde{x}_1/|\tilde{x}_1|$ when $|\tilde{x}_1| > \epsilon_o$ and sat $(\tilde{x}_1, \epsilon_o,) = \tilde{x}_1/\epsilon_o$ when $|\tilde{x}_1| \leq \epsilon_o$. Lastly, $\epsilon_o$ denotes the observer thickness of layer boundary.

Using the estimate of states and perturbation, the RPC for the original system (10) is designed as:

$$\begin{cases} u = b_0^{-1}\left(-\widehat{\Psi}(\cdot) - K(\hat{x} - x^*) + v\right) \\ v = -\phi(y) \end{cases} \tag{16}$$

where $v$ is an additional input $\phi(y)$ is any smooth function satisfying $\phi(0) = 0$ and $y\,\phi(y) > 0$ for all $y \neq 0$, such that the closed-loop system can be transformed into output strictly passive system [32]; and $K = [k_1, k_2, \cdots, k_n]$ is the feedback control gain, which makes matrix $A_1 = A - BK$ Hurwitzian.

## 4. RPC Design of DFIG for Power System Stability Enhancement

It is worth noting that this paper aims to provide a proper active power to enhance power system stability instead of MPPT, in which rotor speed of DFIG should be controlled to extract as much energy as possible from the wind turbine. Hence, rotor speed control is not considered for MPPT.

Choosing the tracking error $e = [e_1 \; e_2]^T$ of active power $P_e$ and reactive power $Q_e$ as the outputs, it yields:

$$\begin{cases} e_1 = P_e - P_e^* \\ e_2 = Q_e - Q_e^* \end{cases} \tag{17}$$

where $P_e^*$ and $Q_e^*$ denote the active power reference and reactive power references, respectively.

Based on the input-output linearization, differentiate tracking error (17) until control inputs $v_{dr}$ and $v_{qr}$ appeared explicitly, gives:

$$\begin{bmatrix} \dot{e}_1 \\ \dot{e}_2 \end{bmatrix} = \begin{bmatrix} f_1 - \dot{P}_e^* \\ f_2 - \dot{Q}_e^* \end{bmatrix} + B \begin{bmatrix} v_{dr} \\ v_{qr} \end{bmatrix} \tag{18}$$

where:

$$\begin{aligned} f_1 &= \omega_b \omega_s \left[ \left( 1 - \frac{\omega_r}{\omega_s} \right) \left( e'_{ds} i_{qs} - e'_{qs} i_{ds} \right) - \frac{1}{\omega_s T_r} \left( e'_{qs} i_{ds} + e'_{ds} i_{ds} \right) \right] \\ &+ \frac{\omega_b}{L'_s} \left[ \frac{\omega_r}{\omega_s} \left( e'^{\,2}_{ds} + e'^{\,2}_{ds} \right) + \omega_s L'_s \left( e'_{qs} i_{ds} - e'_{ds} i_{qs} \right) - R_1 \left( e'_{qs} i_{qs} + e'_{ds} i_{ds} \right) - e'_{qs} v_{qs} \right] \end{aligned} \tag{19}$$

$$\begin{aligned} f_2 &= \frac{\omega_b}{L'_s} \left( \omega_s L'_s i_{qs} + R_1 i_{ds} - \frac{1}{\omega_s T_r} e'_{qs} - \frac{\omega_r}{\omega_s} e'_{ds} \right) v_{qs} \\ &+ \frac{\omega_b}{L'_s} \left( -R_1 i_{qs} + \omega_s L' i_{ds} + \frac{\omega_r}{\omega_s} e'_{qs} - \frac{1}{\omega_s T_r} e'_{ds} - v_{qs} \right) v_{ds} \end{aligned} \tag{20}$$

$$B = \begin{bmatrix} \dfrac{\omega_b L_m}{-2H_m L_{rr}} \left( \dfrac{e'_{ds}}{\omega_s L'_s} - i_{ds} \right) & \dfrac{\omega_b L_m}{-2H_m L_{rr}} \left( \dfrac{e'_{qs}}{\omega_s L'_s} + i_{ds} \right) \\ -\dfrac{\omega_b L_m}{L'_s L_{rr}} v_{qs} & \dfrac{\omega_b L_m}{L'_s L_{rr}} v_{ds} \end{bmatrix} \tag{21}$$

where $f_1$ and $f_2$ include the combinatorial effect of nonlinearties, generator parameter uncertainties, and external disturbances. Moreover, $B$ is the original control gain matrix which elements also contain uncertain generator parameters. Note that their accurate value is very difficult to obtain in practice as generator parameters usually vary along with operation time, temperature, and humidity. As $\det(B) = -\dfrac{\omega_b^2 L_m^2 v_{qs}}{2H_m L'_m L_{rr}^2} \left( \dfrac{e'_{qs}}{\omega_s L_s} + i_{ds} \right) \neq 0$, it is invertible and the transformed system is linearizable over the whole operation range, thus such input-output linearization is always valid.

Assume all the nonlinearities and parameters are unknown, define the perturbations $\psi_1(\cdot)$ and $\psi_2(\cdot)$ for system (18) to aggregate all the nonlinearties, generator uncertainties, and external disturbances of $f_1$, $f_2$, and $B$ into a lumped term, such that they can be rewritten into a concise form, it yields:

$$\begin{bmatrix} \psi_1(\cdot) \\ \psi_2(\cdot) \end{bmatrix} = \begin{bmatrix} f_1 \\ f_2 \end{bmatrix} + (B - B_0) \begin{bmatrix} v_{dr} \\ v_{qr} \end{bmatrix} \tag{22}$$

where the new control gain $B_0$ is given by:

$$B_0 = \begin{bmatrix} b_{11} & 0 \\ 0 & b_{22} \end{bmatrix} \tag{23}$$

where $b_{11}$ and $b_{22}$ are constants. Here, the new control gain $B_0$ is chosen in such form to fully decouple the control of active power and reactive power.

Then system (18) can be rewritten as:

$$\begin{bmatrix} \dot{e}_1 \\ \dot{e}_2 \end{bmatrix} = \begin{bmatrix} \psi_1(\cdot) \\ \psi_2(\cdot) \end{bmatrix} + B_0 \begin{bmatrix} v_{dr} \\ v_{qr} \end{bmatrix} - \begin{bmatrix} \dot{P}_e^* \\ \dot{Q}_e^* \end{bmatrix} \tag{24}$$

Here, the above two first-order differential equations describe the decoupled tracking error dynamics of active power and reactive power, respectively.

A second-order sliding-mode perturbation observer (SMPO) is employed to estimate perturbation $\psi_1(\cdot)$ as:

$$\begin{cases} \dot{\hat{P}}_e = \hat{\psi}_1(\cdot) + \alpha_{11} \tilde{P}_e + k_{11} \mathrm{sat}\left( \tilde{P}_e, \epsilon_o \right) + b_{11} v_{dr} \\ \dot{\hat{\psi}}_1(\cdot) = \alpha_{12} \tilde{P}_e + k_{12} \mathrm{sat}\left( \tilde{P}_e, \epsilon_o \right) \end{cases} \tag{25}$$

where observer gains $k_{11}$, $k_{12}$, $\alpha_{11}$, and $\alpha_{12}$, are all positive constants.

Similarly, another second-order SMPO is used to estimate perturbation $\psi_2(\cdot)$ as:

$$\begin{cases} \dot{\hat{Q}}_e = \hat{\psi}_2(\cdot) + \alpha_{21}\tilde{Q}_e + k_{21}\mathrm{sat}(\tilde{Q}_e, \epsilon_o) + b_{22}v_{qr} \\ \dot{\hat{\psi}}_2(\cdot) = \alpha_{22}\tilde{Q}_e + k_{22}\mathrm{sat}(\tilde{Q}_e, \epsilon_o) \end{cases} \tag{26}$$

where observer gains $k_{21}$, $k_{22}$, $\alpha_{21}$, and $\alpha_{22}$, are all positive constants. The RPC for DFIG system (18) is designed as:

$$\begin{bmatrix} v_{dr} \\ v_{qr} \end{bmatrix} = B_0^{-1}\begin{bmatrix} -\hat{\psi}_1(\cdot) - K_1(\hat{P}_e - P_e^*) + v_1 \\ -\hat{\psi}_2(\cdot) - K_2(\hat{Q}_e - Q_e^*) + v_2 \end{bmatrix} \tag{27}$$

with:

$$\begin{cases} v_1 = -\lambda_1(P_e - P_e^*) \\ v_2 = -\lambda_2(Q_e - Q_e^*) \end{cases} \tag{28}$$

where positive gains $K_1$ and $K_2$ are chosen to ensure the closed-loop system is stable. The energy reshaping coefficients of additional inputs $\lambda_1$ and $\lambda_2$ are carefully selected to inject appropriate system damping into the closed-loop system, such that a satisfactory transient response can be achieved.

To this end, the overall control structure of RPC (27) and (28) for DFIG system (18) is demonstrated by Figure 2. Here, only the measurement of active power $P_e$ and reactive power $Q_e$ is required. At last, the calculated control inputs are modulated by the sinusoidal pulse width modulation (SPWM) technique [33].

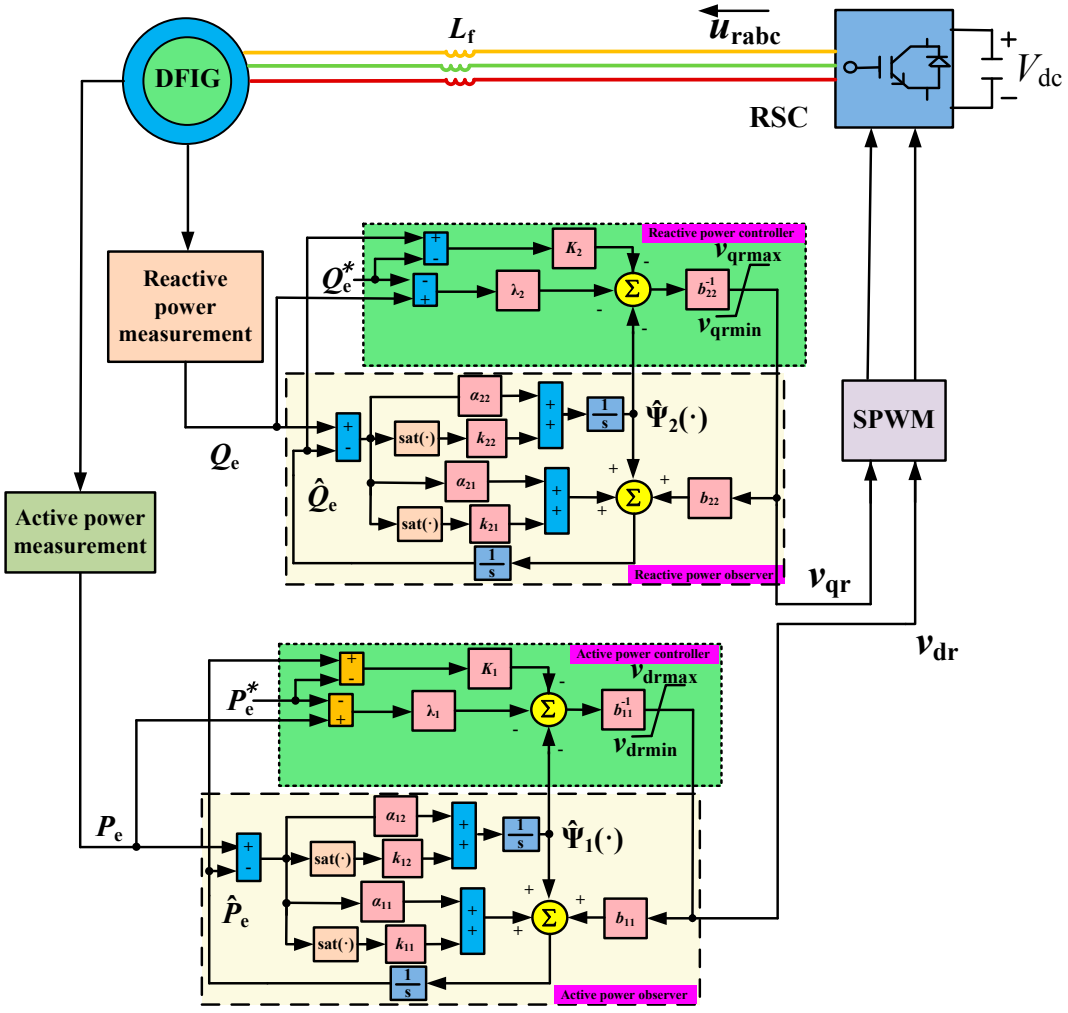


**Figure 2.** The overall RPC structure of DFIG.

## 5. Case Studies

The proposed RPC is applied on DFIG for power system stability enhancement, which control performance is compared to that of conventional PID control [8] and FLC [12], under six scenarios, i.e., (1) Step change of wind speed; (2) Pitch angle variation; (3) Voltage drop at power grid under operation type I; (4) Voltage drop at power grid under operation type II; (5) Inter-area type disturbance; and (6) Generator parameter uncertainties, respectively. Consider the control inputs may exceed the admissible capacity of RSC at some operation point, therefore their values must be limited. Here, $v_{dr}$ and $v_{qr}$ are scaled proportionally as follows: if $v_r = \sqrt{v_{dr}^2 + v_{qr}^2} > v_r^{max}$, then set $v_{dr}^{lim} = v_{dr} v_r^{max}/v_r$ and $v_{qr}^{lim} = v_{qr} v_r^{max}/v_r$ [11]. In addition, the RPC parameters are tabulated in Table 1. The simulation is executed on Matlab/Simulink 7.10 (MathWorks, Natick, MA, USA) using a personal computer with an IntelR CoreTMi7 CPU at 2.2 GHz and 4 GB of RAM.

**Remark 1.** *For the SMPO gains shown in Table 1, they usually range from 10 to 40 to provide a proper trade-off between estimation speed and peak value [26]. A larger observer gain will accelerate the estimation rate but also produce a higher peak value at the moment when system operation condition varies, while a smaller observer gain would not effectively track the output thus degrade the estimation performance significantly. This paper chooses them to be 20 through trial-and-error among this range. For the control gains, they are chosen as so to provide a proper trade-off between the control costs and tracking speed. A too large control gain will rapidly track the output but also result in higher control costs, while a too small control gain might not control the output fast enough but with low control costs. This paper select them to be 30 and 15 for active power and reactive power though trial-and-error, respectively. Note that a fast active power is preferred here as it is important to respond quickly for the purpose of power support.*

**Table 1.** The control parameters of RPC.

| | | | | | |
|---|---|---|---|---|---|
| **Active Power Control Loop** | $b_{11} = -3000$ | $K_1 = 30$ | $\boldsymbol{\lambda_1} = 25$ | $\boldsymbol{\alpha_{11}} = 40$ | $\boldsymbol{\alpha_{12}} = 400$ |
| | $k_{11} = 15$ | $k_{12} = 600$ | $\epsilon_o = 0.2$ | | |
| **Reactive Power Control Loop** | $b_{22} = -4500$ | $K_2 = 15$ | $\lambda_2 = 15$ | $\alpha_{21} = 40$ | $\alpha_{22} = 400$ |
| | $k_{21} = 15$ | $k_{22} = 600$ | | | |

### 5.1. Step Change of Wind Speed

A step change of wind speed from 10 to 12 m/s (10 m/s² rate) with a fixed pitch angle of 15 deg. is tested, the wind speed profile and system responses and control costs are provided in Figure 3. It can be found that PID control presents a 4 s active power oscillation while RPC can effectively supress such unfavourable oscillation in less than 0.5 s, together with the minimal overshoot among all approaches. In addition, RPC needs the least control costs compared to that of PID control and FLC. Although FLC and RPC restore the reactive power slower than that of PID control, they both present a much smoother response with less overshoot.

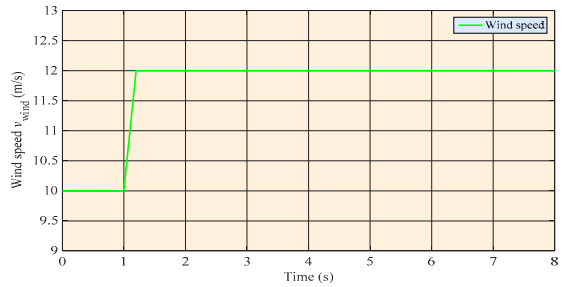


(**a**)Wind speed profile

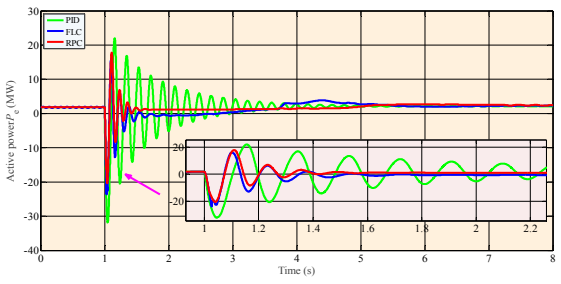


(**b**) Active power

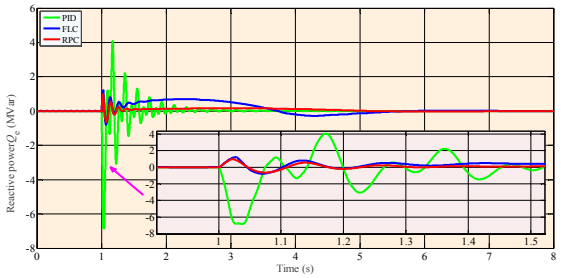


(**c**) Reactive power

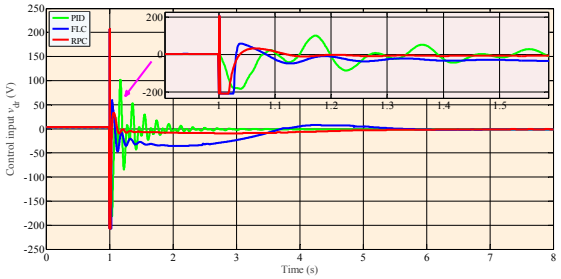


(**d**) d-axis rotor voltage

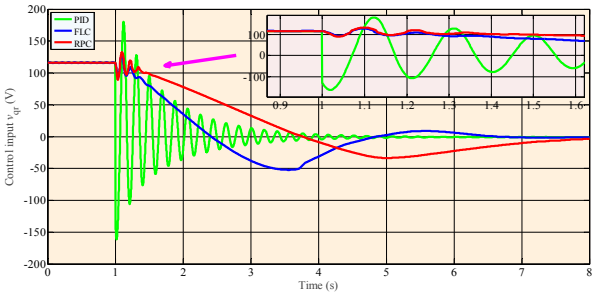


(**e**) q-axis rotor voltage

**Figure 3.** System responses and control costs obtained under a step change of wind speed from 10 to 12 m/s with a fixed pitch angle of 15 deg. (**a**) wind speed profile; (**b**) active power; (**c**) reactive power; (**d**) d-axis rotor voltage; (**e**) q-axis rotor voltage.

### *5.2. Pitch Angle Variation*

A pitch angle reduction that starts from 15 to 5 deg. in 1 s with a constant wind speed of 12 m/s is applied to compare the control performance of RPC against to that of others, while pitch angle is very crucial for the wind power production and secure operation of wind turbine [34]. The system responses are given in Figure 4, which shows that the active power of RPC can converge around 1 s, while FLC and PID control need to consume 1.5 and 3.5 s, respectively. This is due to the extra damping that has been injected via passification. Similar results can be observed in the rotor speed response. As a result, RPC can improve the system damping significantly.

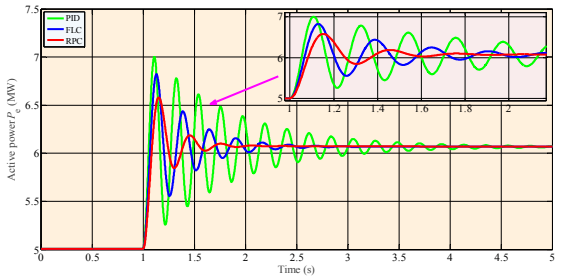


(**a**) Active power

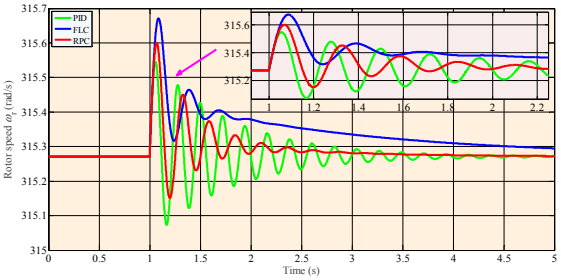


(**b**) Reactive power

**Figure 4.** System responses obtained under a pitch angle variation from 15 to 5 deg. in 1 s with a constant wind speed of 12 m/s. (**a**) active power; (**b**) rotor speed.

### *5.3. Voltage Drop at Power Grid under Operation Type I*

With the high-percentage integration of wind power into the main power grid, it usually requires the wind generator to realize low voltage ride-through (LVRT) when the power grid voltage is temporarily reduced due to a fault or load change in the power grid, or can even address the generator to stay operational and not disconnect from the power grid during and after the voltage dip [35,36]. A 1 s voltage drop starts at $t$ = 1 s from nominal value to 0.65 p.u. and restores to the nominal value, with a constant wind speed of 12 m/s and fixed pitch angle of 15 deg. (operation type I), is applied, while the corresponding system responses are provided by Figure 5. One can

clearly see that a severe high-frequency power oscillation emerges when the fault occurs in PID control which lasts about 0.5 s, such oscillation might deteriorate the power system stability, particularly in the presence of high-percentage wind power penetration. In contrast, RPC can effectively suppress the active and reactive power oscillation with less overshoot and shorter time compared to those of PID control and FLC.

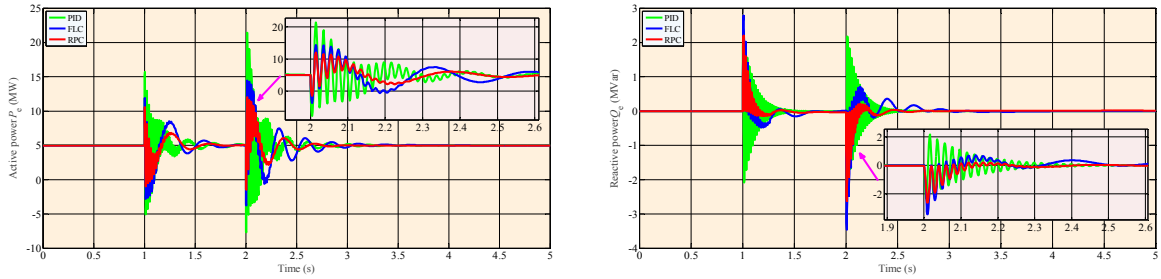


(**a**) Active power (**b**) Reactive power

**Figure 5.** System responses obtained under a 35% voltage drop lasting 1 s at power grid with a constant wind speed of 12 m/s and fixed pitch angle of 15 deg. (operation type I). (**a**) active power; (**b**) reactive power speed.

### *5.4. Voltage Drop at Power Grid under Operation Type II*

In order to investigate the global control consistence of RPC, a 40% voltage drop lasting 1 s at power grid with a constant wind speed of 10 m/s and fixed pitch angle of 5 deg. (operation type II) is applied. The system responses are illustrated in Figure 6, in which a considerable degration of control performance of PID control can be found, this is due to its inherent weakness that the control parameters are determined by the one-point linearization, thus it cannot maintain a consistent control performance or even causes instability when the operation conditions vary. In contrast, both FLC and RPC can achieve a consisitent control performance resulted from the full compensation of system nonlinearities.

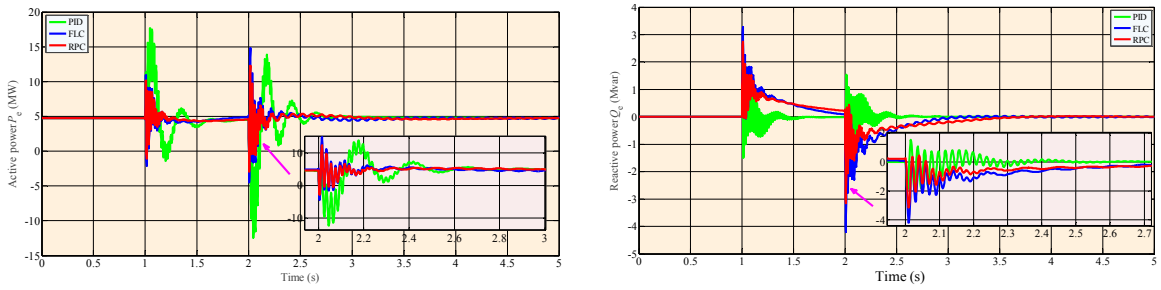


(**a**) Active power (**b**) Reactive power

**Figure 6.** System responses obtained under a 40% voltage drop lasting 1 s at power grid with a constant wind speed of 10 m/s and fixed pitch angle of 5 deg. (operation type II). (**a**) active power; (**b**) reactive power speed.

### *5.5. Inter-Area Type Disturbance*

The low frequency inter-area modes oscillation, which is generally caused by the dynamic interactions in a low frequency (0.1–2.5 Hz) between multiple groups of generators, has been well defined in power system research. It usually results in a degradation of power system stability and must be effectively suppressed [37]. It is of concern that the single machine infinite bus (SMIB)-designed controller may not perform well in the presence of inter-area modes oscillation. As a consequence, it is necessary to evaluate the SMIB-designed RPC on a more realistic multi-machine power system model with different oscillation frequencies. One approach called single machine quasi-infinite bus, where the infinite bus of the main power grid is modulated in magnitude by

inter-area-type frequencies [16]. An inter-area type disturbance $v_s = 1 + 0.1 \sin(\pi t/1.25)$ is chosen to a corresponding oscillation frequency of 0.4 Hz.

System responses are given in Figure 7, the control performance of both PID control and FLC degrades due to this unknown external disturbance. In contrast, RPC can effectively attenuate the inter-area disturbance as such external disturbance can be rapidly estimated and compensated in real-time.

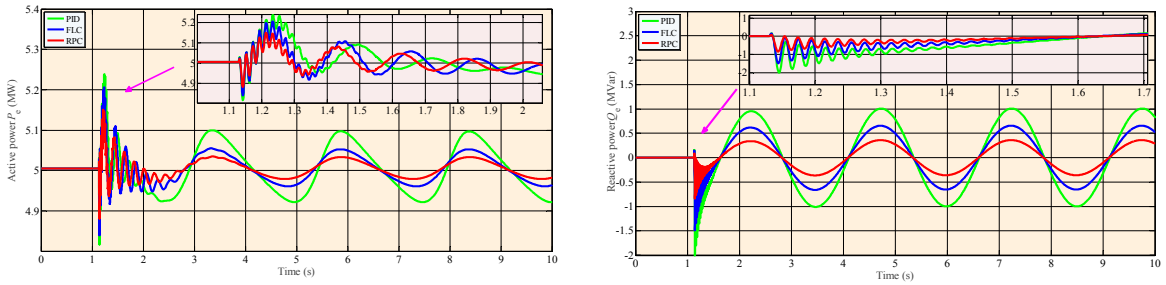


(**a**) Active power (**b**) Reactive power

**Figure 7.** System responses obtained under an inter-area type disturbance $v_s = 1 + 0.1 \sin(\pi t/1.25)$. (**a**) active power; (**b**) reactive power speed.

### *5.6. Generator Parameter Uncertainties*

In order to evaluate the robustness against to generator parameter uncertainties, a series of plant-model mismatches of stator resistance $R_s$ and mutual inductance $L_m$ with ±20% variation around their nominal value are undertaken, in which a 0.2 p.u. voltage drop for 0.1 s at power grid is applied. The peak value of active power $|P_e|$ is recorded for a clear comparison. Figure 8 demonstrates that the variation of $|P_e|$ obtained by PID control, FLC, and RPC is 10.2%, 22.4%, 5.3%, respectively. It is worth noting that FLC requires the full state measurement and the accurate system model, thus it is highly invulnarable to any modelling uncertainties. In contrast, PID control and RPC do not need an accurate system model hence they are more robust to parameter uncertainties. Since RPC can compensate the parameter uncertainties, it has the strongest robustness among all approaches.

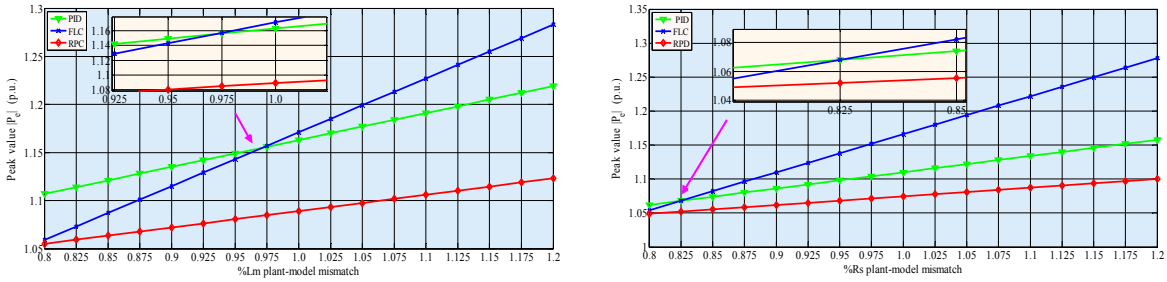


(**a**) Mutual inductance mismatch (**b**) Stator resistance mismatch

**Figure 8.** Peak value of active power $|P_e|$ obtained under a 0.2 p.u. voltage drop lasting 0.1 s at power grid with 20% variation of the stator resistance $R_s$ and mutual inductance $L_m$ of three approaches, respectively. (**a**) mutual inductance mismatch; (**b**) stator resistance mismatch.

### *5.7. Comparative Studies*

The integral of absolute error (IAE) indices of each controller calculated in five scenarios are presented in Table 2, where $\text{IAE}_x = \int_0^T |x - x^*| \, dt$. The simulation time $T$ = 10 s. It shows that RPC owns the lowest IAE indices of active power (in bold) in all scenarios. In particular, its $\text{IAE}_{Pe}$ obtained in step change of wind speed is merely 20.97% and 65.55% to that of PID control and FLC, respectively.

**Table 2.** IAE indices of different controllers obtained in different scenarios (p.u.).

| Case | Step Change of Wind Speed | Pitch Angle Variation | Voltage Drop of Type I | Voltage Drop of Type II | Inter-Area Type Disturbance |
|---|---|---|---|---|---|
| Controller | IAE index $IAE_{Pe}$ of active power | | | | |
| PID | 1.216 | 1.072 | 2.166 | 1.986 | 0.855 |
| FLC | 0.389 | 0.633 | 1.459 | 1.269 | 0.516 |
| RPC | **0.255** | **0.529** | **1.287** | **1.138** | **0.429** |
| Controller | IAE index $IAE_{Qe}$ of reactive power | | | | |
| PID | 0.752 | 0.951 | **0.896** | 0.589 | 0.917 |
| FLC | 0.689 | **0.708** | 1.016 | 0.354 | 0.639 |
| RPC | **0.611** | 0.895 | 0.987 | **0.317** | **0.528** |

Finally, the overall control costs of these three controllers acquired in five scenarios are compared in Table 3. Here, RPC needs the lowest control costs in step change of wind speed, pitch angle variation, and voltage drop of type II. Furthermore, it ranks the seond-lowest in voltage drop of type I and inter-area type disturbance, which just needs similar control costs to that of FLC (the lowest one). To summarize, RPC outperforms PID control and FLC with globally consistent control performance under various operation conditions, strongest robustness against to generator parameter uncertainties, and reasonable control costs.

**Table 3.** Overall control costs of different controllers obtained in different scenarios (p.u.).

| Case (Controller) | Step Change of Wind Speed | Pitch Angle Variation | Voltage Drop of Operation Type I | Voltage Drop of Operation Type II | Inter-Area Type Disturbance |
|---|---|---|---|---|---|
| PID | 0.274 | 0.217 | 0.469 | 0.371 | 0.257 |
| FLC | 0.209 | 0.165 | **0.388** | 0.297 | **0.226** |
| RPC | **0.187** | **0.148** | 0.392 | **0.285** | 0.231 |

## 6. Conclusions

In this paper, a model-free RPC scheme is designed for DFIG to enhance the power system stability. The main contributions and key findings of this paper can be summarized in the following four aspects:

(1) A nonlinear observer is employed to estimate the aggregated effect of generator nonlinearities and parameter uncertainties, unmodelled dynamics, and wind speed randomness, which is then fully compensated in real-time by a passive controller. Hence, RPC can handle various types of uncertainties which is applicable to more practical cases compared to that of parameter based robust/adaptive approaches;
(2) An extra damping is injected to improve system transient dynamics via energy reshaping, which can provide a faster active power response when DFIG is disturbed thus the power system stability could be enhanced significantly;
(3) RPC does not require an accurate system model while only the measurement of active power and reactive power is required. Therefore, RPC is very easy to be implemented in practice;
(4) Simulation results demonstrate that RPC can maintain a globally consistent control performance in the face of varied pitch angle, wind speed, voltage drop at power grid, and inter-area type disturbance. Compared to PID control and FLC, RPC can effectively suppress the active power and reactive power oscillation while reduce the overshoot simultaneously, such that the power system stability can be considerably enhanced. Furthermore, it just needs reasonable control costs.

Future studies will be focused on the following three aspects: (1) examine RPC for GSC to accomplish an overall control system design and test its implementation feasibility in a multi-machine power system through real-time digital simulator (RTDS); (2) employ optimization algorithms, e.g., GA or PSO, to optimize the gains selection procedure of SMPO and RPC; (3) adopt RPC in a real-time digital simulator (RTDS) to validate its implementation feasibility.

**Acknowledgments:** The authors gratefully acknowledge the support of National Natural Science Foundation of China (51667010) and Project on Adaptability of Renewable Energy to Power Grid and Key Detection Technologies under Asynchronous Network of Yunnan Power Grid (YNKJQQ00000279).

**Author Contributions:** Preparation of the manuscript has been performed by Jun Dong, Shengnan Li, Shuijun Wu, Tingyi He, Bo Yang, Hongchun Shu and Jilai Yu.

**Conflicts of Interest:** The authors declare no conflict of interest.

## Nomenclature

**Variables**

| | |
|---|---|
| $v_{wind}$ | wind velocity |
| $\rho$ | air density |
| $R$ | turbine radius |
| $C_P$ | power coefficient |
| $C_{Pmax}$ | maximum power coefficient |
| $\lambda$ | tip-speed-ratio |
| $\lambda_{opt}$ | optimal tip-speed-ratio |
| $\beta$ | blade pitch angle |
| $T_e$ | electromagnetic torque |
| $T_m$ | mechanical torque |
| $Q_s$ | reactive power |
| $s$ | generator slip |
| $\omega_s$ | synchronous angle speed |
| $\omega_r$ | rotor angular speed |
| $\omega_b$ | electrical base speed |
| $i_{dr}$, $i_{qr}$ | dq-axis rotor current |
| $i_{ds}$, $i_{qs}$ | dq-axis stator current |

**System Parameters**

| | |
|---|---|
| $\sigma$ | leakage coefficient |
| $R_s$,$R_r$ | stator and rotor resistances |
| $L_s$,$L_r$ | stator and rotor inductances |
| $L_m$ | magnetizing inductance |
| $H_g$ | generator inertia |
| $H_t$ | turbine inertia |
| $D$ | damping coefficient |

**Abbreviations**

| | |
|---|---|
| DFIG | doubly fed induction generator |
| RPC | robust passive control |
| ESO | extended state observer |
| RSC | rotor side converter |
| PSO | particle swarm optimizer |
| MPPT | maximum power point tracking |
| GGWO | grouped grey wolf optimizer |
| SMC | sliding-mode control |
| PC | passive control |
| DG | distributed generators |
| SMSPO | sliding-mode state and perturbation observer |
| GSC | grid side converter |
| SPWM | sinusoidal pulse width modulation |
| LVRT | low voltage ride-through |
| SMIB | single machine infinite bus |
| PID | proportional-integral-derivative |
| FLC | feedback linearization control |
| GA | genetic algorithm |

**The Control Parameters of RPC**

| | |
|---|---|
| $k_{11}$ | SMPO sliding-mode gain of active power |
| $k_{12}$ | SMPO sliding-mode gain of active power |
| $\alpha_{11}$ | SMPO gain of active power |
| $\alpha_{12}$ | SMPO gain of active power |
| $k_{21}$ | SMPO sliding-mode gain of reactive power |
| $k_{22}$ | SMPO sliding-mode gain of reactive power |
| $\alpha_{21}$ | SMPO gain of reactive power |
| $\alpha_{22}$ | SMPO gain of reactive power |
| $K_1$ | control gain of active power |
| $K_2$ | control gain of reactive power |
| $\lambda_1$ | reshaping coefficient of active power |
| $\lambda_2$ | reshaping coefficient of reactive power |

## Appendix A

### *Appendix A.1. System Parameters*

$\omega_b = 100\pi$ rad/s, $\omega_s = 1.0$ p.u., $\omega_{r\_base} = 1.29$ p.u., $v_{s\_norm} = 1.0$ p.u.

### *Appendix A.2. DFIG Parameter*

$P_{rated} = 10$ MW, $R_s = 0.005$ p.u., $L_m = 4.0$ p.u., $R_r = 1.1R_s$, $L_{ss} = 1.0L_m$, $L_{rr} = 1.005L_{ss}$, $L'_s = L_{ss} - \frac{L_m^2}{L_{rr}}$, $T_r = L_{rr}/R_r$, $R_1 = R_s + R_2$, $R_2 = (L_m/L_{rr})^2 R_r$.

### *Appendix A.3. Wind Turbine Parameters*

$\rho = 1.225$ kg/m$^3$, $R = 58.59$ m$^2$, $v_{wind\_norm} = 15$ m/s, $\lambda_{opt} = 6.325$, $H_m = 4.4$ s, $\beta_{norm} = 15$ deg.

## References

1. Sun, X.; Zhang, B.; Tang, X.; McLellan, B.C.; Höök, M. Sustainable energy transitions in China: Renewable options and impacts on the electricity system. *Energies* **2016**, *9*, 980.
2. Boroojeni, K.G.; Amini, M.H.; Nejadpak, A.; Iyengar, S.S.; Hoseinzadeh, B.; Bak, C.L. A theoretical bilevel control scheme for power networks with large-scale penetration of distributed renewable resources. *IEEE Int. Conf. Electro Inf. Technol.* **2016**, 510–515.
3. Amini, M.H.; Nabi, B.; Haghifam, M.R. Load management using multi-agent systems in smart distribution network. In Proceedings of the 2013 IEEE Power and Energy Society General Meeting (PES), Vancouver, BC, Canada, 21–25 July 2013.
4. Hooper, T.; Beaumont, N.; Hattam, C. The implications of energy systems for ecosystem services: A detailed case study of offshore wind. *Renew. Sustain. Energy Rev.* **2017**, *70*, 230–241.
5. Zuo, J.; Li, Y.H.; Shi, D.Y.; Duan, X.Z. Simultaneous robust coordinated damping control of power system stabilizers (PSSs), static var compensator (SVC) and doubly-fed induction generator power oscillation dampers (DFIG PODs) in multimachine power systems. *Energies* **2017**, *10*, 565.
6. Vahdati, P.M.; Vanfretti, L.; Amini, M.H. Hopf bifurcation control of power systems nonlinear dynamics via a dynamic state feedback controller-Part I: Theory and modelling. *IEEE Trans. Power Syst.* **2017**, *32*, 3217–3228.
7. Boroojeni, K.G.; Amini, M.H.; Iyengar, S.S. *Smart Grids: Security and Privacy Issues*; Springer International Publishing: Cham, Switzerland, 2017.
8. Li, S.H.; Haskew, T.A.; Williams, K.A.; Swatloski, R.P. Control of DFIG wind turbine with direct-current vector control configuration. *IEEE Trans. Sustain. Energy* **2012**, *3*, 1–11.
9. Barros, L.S.; Mota, W.S.; Silveira; L.G.Q.; Oliveira, P.S. DFIG rotor side control through gain-scheduling designed by genetic algorithm. In Proceedings of the 2012 Sixth IEEE/PES Transmission and Distribution: Latin America Conference and Exposition (T&D-LA), Montevideo, Uruguay, 3–5 September 2012; pp. 1–6.
10. Bekakra, Y; Attous, D.B. Optimal tuning of PI controller using PSO optimization for indirect power control for DFIG based wind turbine with MPPT. *Int. J. Syst. Assur. Eng. Manag.* **2014**, *5*, 219–229.
11. Yang, B.; Zhang, X.S.; Yu, T.; Shu, H.C.; Fang, Z.H. Grouped grey wolf optimizer for maximum power point tracking of doubly-fed induction generator based wind turbine. *Energy Convers. Manag.* **2017**, *133*, 427–443.
12. Yang, B.; Jiang, L.; Wang, L.; Yao, W.; Wu, Q.H. Nonlinear maximum power point tracking control and modal analysis of DFIG based wind turbine. *Int. J. Electr. Power Energy Syst.* **2016**, *74*, 429–436.
13. Benbouzid, M.; Beltran, B.; Amirat, Y.; Yao, G.; Han, J.G.; Mangel, H. Second-order sliding mode control for DFIG-based wind turbines fault ride-through capability enhancement. *ISA Trans.* **2014**, *53*, 827–833.
14. Tan, A.G.; Lin, X.N.; Sun, J.W.; Ran, L.Y.; Li, Z.T.; Long, P.; Muhammad, S.K. A novel DFIG damping control for power system with high wind power penetration. *Energies* **2016**, *9*, 521.
15. Ataji, A.B.; Miura, Y.; Ise, T.; Tanaka, H. A new robust decoupled control of the stator active and reactive currents for grid-connected doubly-fed induction generators. *Energies* **2016**, *9*, 179.
16. Yang, B.; Jiang, L.; Yao, W.; Wu, Q.H. Perturbation estimation based coordinated adaptive passive control for multimachine power systems. *Control Eng. Pract.* **2015**, *44*, 172–192.
17. Ortega, R.; Schaf, A.; Castanos, F.; Astolfi, A. Control by interconnection and standard passivity-based control of port-Hamiltonian systems. *IEEE Trans. Autom. Control* **2008**, *53*, 2527–2542.
18. Molavi, A.; Jalali, A.; Naraghi, M.G. Adaptive fuzzy control of a class of nonaffine nonlinear system with input saturation based on passivity theorem. *ISA Trans.* **2017**, *69*, 202–213, doi:10.1016/j.isatra.2017.03.020.
19. Koeln, J.P.; Alleyne, A.G. Stability of decentralized model predictive control of graph-based power flow systems via passivity. *Automatica* **2017**, *82*, 29–34.
20. Wen, H.; Chen, T.; Jin, D.P.; Hu, H.Y. Passivity-based control with collision avoidance for a hub-beam spacecraft. *Adv. Space Res.* **2017**, *59*, 425–433.
21. Donaire, A.; Ortega, R.; Romero, J.G. Simultaneous interconnection and damping assignment passivity-based control of mechanical systems using dissipative forces. *Syst. Control Lett.* **2016**, *94*, 118–126.
22. Azimi, S.M.; Afsharnia, S. Multi-purpose droop controllers incorporating a passivity-based stabilizer for unified control of electronically interfaced distributed generators including primary source dynamics. *ISA Trans.* **2016**, *63*, 140–153.
23. Li, Q.; Zhang, Q.L.; Yi, N.; Yuan, Y.H. Robust passive control for uncertain time-delay singular systems. *IEEE Trans. Circuits Syst. I Regul. Pap.* **2009**, *56*, 653–663.

24. Wu, Z.G.; Shi, P.; Su, H.Y.; Chu, J. Network-based robust passive control for fuzzy systems with randomly occurring uncertainties. *IEEE Trans. Fuzzy Syst.* **2013**, *21*, 966–971.
25. Ma, Y.C.; Yang, P.J.; Yan, Y.F.; Zhang, Q.L. Robust observer-based passive control for uncertain singular time-delay systems subject to actuator saturation. *ISA Trans.* **2017**, *67*, 9–18.
26. Yang, B.; Sang, Y.Y.; Shi, K.; Yao, W.; Jiang, L.; Yu, T. Design and real-time implementation of perturbation observer based sliding-mode control for VSC-HVDC systems. *Control Eng. Pract.* **2016**, *56*, 13–26.
27. Fei, M.; Pal, B. Modal analysis of grid-connected doubly fed induction generators. *IEEE Trans. Energy Convers.* **2007**, *22*, 728–736.
28. Qiao, W. Dynamic modeling and control of doubly fed induction generators driven by wind turbines. In Proceedings of the IEEE/PES Power Systems Conference and Exposition, Seattle, WA, USA, 15–18 March 2009; pp. 1–8.
29. Liu, Y.; Wu, Q.H.; Zhou, X.X.; Jiang, L. Perturbation observer based multiloop control for the DFIG-WT in multimachine power system. *IEEE Trans. Power Syst.* **2014**, *29*, 2905–2915.
30. Jiang, L. Nonlinear Adaptive Control and Applications in Power Systems. Ph.D. Thesis, University of Liverpool, Liverpool, UK, 2001.
31. Jiang, L.; Wu, Q.H.; Wen, J.Y. Nonlinear adaptive control via sliding-mode state and perturbation observer. *IEE Proc. Control Theory Appl.* **2002**, *149*, 269–277.
32. Khalil, H. *Nonlinear Systems*; Prentice Hall: Upper Saddle River, NJ, USA, 2001.
33. Juan, R.; Edgar, L.; Vicente, V.; David, C.; Ramon, A.; Luis, E. Current-sensorless control of an SPWM H-Bridge-based PFC rectifier designed considering voltage sag condition. *Electr. Power Syst. Res.* **2016**, *130*, 181–191.
34. Duong, M.Q.; Grimaccia, F.; Leva, S.; Mussetta, M.; Ogliari, E. Pitch angle control using hybrid controller for all operating regions of SCIG wind turbine system. *Renew. Energy* **2014**, *70*, 197–203.
35. Saad, N.H.; Sattar, A.A.; Mansour, A.E.M. Low voltage ride through of doubly-fed induction generator connected to the grid using sliding mode control strategy. *Renew. Energy* **2015**, *80*, 583–594.
36. Rashid, G.; Ali, M.H. Nonlinear control-based modified BFCL for LVRT capacity enhancement of DFIG-based wind farm. *IEEE Trans. Energy Convers.* **2017**, *32*, 284–295.
37. Yao, W.; Jiang, L.; Wen, J.Y.; Wu, Q.H.; Cheng, S.J. Wide-area damping controller for power system inter-area oscillations: A networked predictive control approach. *IEEE Trans. Control Syst. Technol.* **2015**, *23*, 27–36.